Preparation-based B1+ mapping in the heart using Bloch–Siegert shifts

Šiurytė, Paulina; Tourais, Joao; Zhang, Yi; Coletti, Chiara; van de Steeg-Henzen, Christal; Mandija, Stefano; Tao, Qian; Henningsson, Markus; Weingärtner, Sebastian

DOI
10.1002/mrm.30232

Publication date
2024

Document Version
Final published version

Published in
Magnetic Resonance in Medicine

Received: 20 March 2024 | Revised: 11 June 2024 | Accepted: 10 July 2024

DOI: 10.1002/mrm.30232

Magnetic Resonance in Medicine

TECHNICAL NOTE

Preparation-based B_1^+ mapping in the heart using Bloch–Siegert shifts

Paulina Šiurytė[1] | Joao Tourais[1] | Yi Zhang[1] | Chiara Coletti[1] | Christal van de Steeg-Henzen[2] | Stefano Mandija[3] | Qian Tao[1] | Markus Henningsson[4] | Sebastian Weingärtner[1,2]

[1]Department of Imaging Physics, Delft University of Technology, Delft, The Netherlands

[2]HollandPTC, Delft, The Netherlands

[3]Department of Radiotherapy, Division of Imaging & Oncology, University Medical Center Utrecht, Utrecht, The Netherlands

[4]Department of Health, Medicine and Caring Sciences, Linköping University, Linköping, Sweden

Correspondence
Sebastian Weingärtner, Department of Imaging Physics, Delft University of Technology, Lorentzweg 1, 2628 CJ Delft, The Netherlands.
Email: s.weingartner@tudelft.nl

Funding information
European Research Council, Grant/Award Number: 101078711; Nederlandse Hartstichting, Grant/Award Number: 03-004-2022-0079; Nederlandse Organisatie voor Wetenschappelijk Onderzoek, Grant/Award Number: STU.019.024; 4TU Precision Medicine program supported by High Tech for a Sustainable Future

Abstract

Purpose: To develop and evaluate a robust cardiac B_1^+ mapping sequence at 3 T, using Bloch–Siegert shift (BSS)-based preparations.

Methods: A longitudinal magnetization preparation module was designed to encode $|B_1^+|$. After magnetization tip-down, off-resonant Fermi pulses, placed symmetrically around two refocusing pulses, induced BSS, followed by tipping back of the magnetization. Bloch simulations were used to optimize refocusing pulse parameters and to assess the mapping sensitivity. Relaxation-induced B_1^+ error was simulated for various T_1/T_2 times. The effective mapping range was determined in phantom experiments, and $|B_1^+|$ maps were compared to the conventional BSS method and subadiabatic hyperbolic-secant 8 (HS8) pulse-sensitized method. Cardiac B_1^+ maps were acquired in healthy subjects, and evaluated for repeatability and imaging plane intersection consistency. The technique was modified for three-dimensional (3D) acquisition of the whole heart in a single breath-hold, and compared to two-dimensional (2D) acquisition.

Results: Simulations indicate that the proposed preparation can be tailored to achieve high mapping sensitivity across various B_1^+ ranges, with maximum sensitivity at the upper B_1^+ range. T_1/T_2-induced bias did not exceed 5.2%. Experimentally reproduced B_1^+ sensitization closely matched simulations for $B_1^+ \geq 0.3B_{1,\max}^+$ (mean difference 0.031±0.022, compared to 0.018±0.025 in the HS8-sensitized method), and showed 20-fold reduction in the standard deviation of repeated scans, compared with conventional BSS B_1^+ mapping, and an equivalent 2-fold reduction compared with HS8-sensitization. Robust cardiac B_1^+ map quality was obtained, with an average test-retest variability of 0.027±0.043 relative to normalized B_1^+ magnitude, and plane intersection bias of 0.052±0.031. 3D acquisitions showed good agreement with 2D scans (mean absolute deviation 0.055±0.061).

Conclusion: BSS-based preparations enable robust and tailorable 2D/3D cardiac B_1^+ mapping at 3 T in a single breath-hold.

KEYWORDS

B_1^+ mapping, Bloch–Siegert shift, cardiac imaging, preparation-based

Markus Henningsson and Sebastian Weingärtner contributed equally to this work.

1 | INTRODUCTION

Cardiac MR imaging at high magnetic fields (≥3 T) is commonly used due to the promise of increased signal-to-noise ratios compared to 1.5 T.[1,2] However, body imaging at high magnetic fields suffers from strong inhomogeneities of the transmitted radiofrequency (RF) field B_1^+.[3–5] The inhomogeneities arise as RF wavelengths approach the body dimensions, leading to dielectric artifacts causing inadvertent areas of low/high contrast. In cardiac imaging, flip-angle variations reach up to 50% across the area of interest,[6,7] compromising both qualitative image reading, and quantitative measurements.[8,9]

B_1^+ mapping is routinely used for inhomogeneity compensation with shimming[10] or for correction of quantitative measurements.[11] However, the application of most B_1^+ mapping approaches to the heart is complicated by cardiac and respiratory motion. The saturated double angle method) has been previously applied in cardiac MR,[12] although with limited visual mapping quality. Bloch–Siegert shift (BSS) mapping has shown promise for motion-robust cardiac B_1^+ mapping.[13,14] Here an off-resonant pulse is played after each excitation to accrue a $|B_1^+|$-dependent phase shift.[15] However, this requires long echo times (TE) making the acquisition sensitive to off-resonances, especially in the presence of implanted devices or other sources of susceptibility.

Preparation-based B_1^+ mapping methods, such as stimulated echo acquisition mode,[16] or presaturation TurboFLASH[17] have also been explored in cardiac imaging. These offer specific absorption rate (SAR)-efficiency and are promising for fast mapping. Stimulated echo acquisition mode-based dual refocusing echo acquisition mode has been applied to myocardial B_1^+ mapping, but the map quality is limited by the use of echo planar imaging readouts.[18] Furthermore, sensitivity to flow hinders B_1^+ mapping in the ventricular blood pools. A presaturation TurboFLASH method has achieved robust whole heart mapping.[19] However, with previously proposed sinc or subadiabatic HS pulses, the method is less sensitive at higher relative B_1^+ power, which is commonly the range of interest.

In this work, we investigate the use of BSS in longitudinal magnetization preparations for tailored $|B_1^+|$ sensitivity, combined with snap-shot imaging for robust and efficient B_1^+ mapping of the heart. The sensitivity, quantification bias, and precision of the proposed preparation-based mapping method were assessed in Bloch simulations and phantom experiments. In vivo B_1^+ mapping is evaluated in a cohort of healthy subjects and compared to conventional BSS mapping and the subadiabatic pulse HS8-sensitized method. Finally, the feasibility of whole-heart, single breath-hold B_1^+ mapping is demonstrated.

2 | METHODS

2.1 | B_1^+ preparation module and mapping sequence

The proposed B_1^+ mapping method uses a preparation module that sensitizes the longitudinal magnetization to a $|B_1^+|$-dependent BSS. The module consists of a tip-down/tip-up pulse pair surrounding four off-resonant pulses, placed symmetrically around two refocusing pulses (Figure 1). After the magnetization is tipped by the initial $90^\circ_{0^\circ}$ hard pulse (with underscore indicating the pulse phase), it accumulates $\pm\phi_{BS}$ phase during each of the four off-resonant pulses (Figure 1A). This results in a reduced magnetization component along the tip-back axis, depending on the cosine of the accrued phase. The B_1^+-sensitized magnetization is then tipped up with a $90^\circ_{180^\circ+\phi_{TB}}$ hard pulse. The tip-back phase offset ϕ_{TB} can be used to tailor the sensitivity to various B_1^+ ranges. Finally, a spoiler gradient is applied (duration 6.25 ms) to eliminate residual transverse magnetization.

For B_1^+ mapping, three images are acquired to extract the BSS-weighted image contrast in a confounder-resilient manner (Figure 1B):

1. $I_{4\phi}$ image with cumulative 4ϕ phase;
2. $I_{0\phi}$ equivalent image with a zero BSS is achieved by selectively flipping the off-resonance pulse frequency shift polarity (BS+ and BS−), to compensate for relaxation and magnetization transfer;
3. I_{sat} image preceded by "Water suppression Enhanced through T_1-effects" saturation pulse, to compensate for the effect of the snap-shot readout.[20]

The ratio of the prepared images can be expressed as:

$$\frac{M_{4\phi}}{M_{0\phi}} = \frac{I_{4\phi} - I_{sat}}{I_{0\phi} - I_{sat}} \tag{1}$$

$$= \frac{\sin^2(90^\circ\beta)\ \cos(4\kappa_{BS}(B_{1,max}^+\beta)^2)\ +\ \cos^2(90^\circ\beta)}{\sin^2(90^\circ\beta)\ +\ \cos^2(90^\circ\beta)}. \tag{2}$$

Here β describes the normalized transmit field magnitude ($B_{1,norm}^+$), $B_{1,max}^+$ is the Fermi pulse amplitude and κ_{BS} is the pulse-shape dependent scaling constant.[15] $B_{1,norm}^+$ maps are generated by β parameter voxel-wise fitting of Equation (2) using a golden section search-based optimization via Matlab (Mathworks). Perfect refocusing was assumed during the reconstruction.

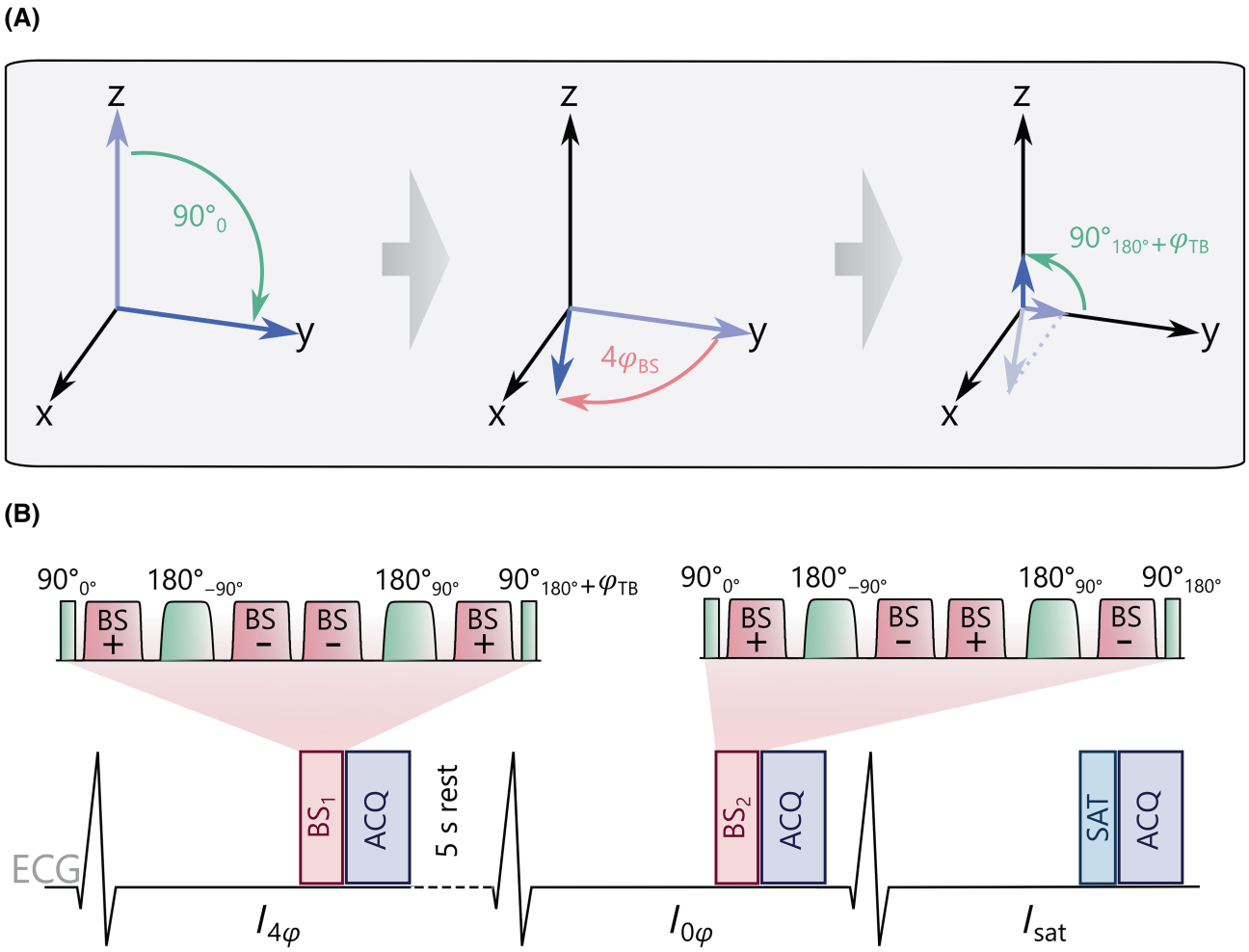

FIGURE 1 (A) Schematic of the magnetization evolution during the Bloch–Siegert shift (BSS) preparation during the tip-down (left), during the 4ϕ $|B_1^+|$-dependent phase shift (middle), and the tip-up with reduced transverse magnetization component along the tip-back phase ϕ_{TB} (right). (B) BSS-based preparation modules with effective BSS phase shift of 4ϕ (BS_1) and effective phase shift of 0 (BS_2). Both preparations contain tipping and refocusing pulses (green) and off-resonant Fermi pulses (pink), with variable polarity (plus/minus) of the frequency offset. Below is the sequence diagram of three baseline images ($I_{4\phi}$, $I_{0\phi}$, I_{sat}) required for confounder-resilient B_1^+ map reconstruction. End-diastole imaging (ACQ) is preceded by the preparation module or saturation preparation (SAT). A rest period is played for longitudinal magnetization recovery before the $I_{0\phi}$ image, and all images are acquired in a single breath hold. (A) Magnetization evolution; (B) Sequence diagram.

Off-resonant pulses were played at ±7 kHz offset, and a Fermi shape with a full-width-half-maximum of 90% ($\kappa_{BS} = 7.28 \cdot 10^8$ rad/ms). Refocusing was performed using adiabatic tanh/tan pulses placed equidistantly between the tip-down and tip-up pulses.

For cardiac $|B_1^+|$ mapping, single breath-hold, end-diastolic electrocardiogram (ECG)-triggered images were acquired with a 5-s rest period between the BSS-prepared images for longitudinal magnetization recovery (Figure 1B).

2.2 | Simulations

Simulations were performed to optimize the Fermi pulse duration d_{BS} for maximum mapping sensitivity and bijective B_1^+ encoding. For a tip-back phase of $\phi_{TB} = 0$, BSS of 180° was specified at the maximum expected $|B_1^+|$ value. Based on previous literature, 110% of the nominal RF amplitude was chosen for 3 T.[7] Refocusing pulse duration d_{REF} and shape parameters ξ and f_{max} were optimized to yield high B_0/B_1^+ resilience at $B_{1,norm}^+ \in [0.5,1.1]$ and off-resonance $\Delta\omega \in [-200,200]$ Hz using Bloch simulations of the preparation with $\phi_{BS} = 0$. $B_{1,max}^+$ of 13.5 μT was used for RF pulses to match the scanner hardware limitations.

The B_1^+ sensitivity of the proposed preparation was assessed using Bloch simulations for $B_{1,norm}^+ \in [0,1.1]$, and compared to subadiabatic HS8 preparation, as previously used in B_1^+ mapping.[19] The B_1^+ sensitivity was obtained as the derivative of the postpreparation longitudinal

magnetization with respect to $B^+_{1,norm}$. HS8 pulses were simulated with a time-bandwidth product of 15 and a truncating factor of 5.3.[19,21,22] For the proposed preparation, 45 ms sequence duration, $d_{BS} = 4.6$ ms and $\phi_{TB} = 0$ parameters were used.

To assess the impact of residual relaxation effects, the B^+_1 error was estimated for various T_1 and T_2 combinations: $T_1 \in \{250; 1500\}$ ms and $T_2 \in \{50{,}100, 150\}/\{50{,}150, 250\}$ ms. The postpreparation magnetization was simulated using Bloch simulations including or excluding T_1 and T_2 relaxation effects. The error was estimated as the relative difference in the obtained $B^+_{1,norm}$ values. The preparation parameters were simulated as listed above.

2.3 | Imaging

Experiments were performed on a 3 T Philips Ingenia scanner without first-level SAR mode. For two-dimensional (2D) mapping, the proposed method used 45–50 ms preparation (unless stated otherwise), followed by a snap-shot balanced steady-state free precession readout. Imaging was performed with flip angle = 40°, bandwidth BW = 1447 Hz/px, slice thickness $s = 10$ mm and matrix size = 120 × 120. In the preparation, $d_{REF} = 4$ ms refocusing pulses with $\xi = 8$ and $f_{max} = 5400$ Hz were used. Fermi pulse duration was $d_{BS} = 4.6$ ms unless stated otherwise.

2.4 | Phantom experiments

To demonstrate the mapping sensitivity tailoring to different $B^+_{1,norm}$ ranges, three different BSS-preparations were designed. The tip-down/up angle, the Fermi pulse duration d_{BS} and the tip-back phase ϕ_{TB} of the BSS-prepared image with 4ϕ shift were chosen, based on simulations, to achieve peak sensitivity at $B^+_{1,P,norm} = 0.7/0.8/0.9$, respectively. The preparations were performed with a duration of 65 ms and Fermi pulse amplitude of $B_{1,max} = 13.5$ μT. Phantom scans were performed in the T1MES phantom[23] with FOV = 300 × 300 mm^2, $s = 10$ mm, TR/TE = 2.5/1.2 ms, and seven repetitions. To simulate B^+_1 inhomogeneities, the power of the RF pulses in the preparation was scaled between $B^+_{1,P,norm}$ −0.25 and $B^+_{1,P,norm}$+0.05 in steps of 0.05. The SD of the reconstructed $B^+_{1,norm}$ values, mapped in a manually drawn region of interest (ROI) of the central phantom vial (T_1/T_2 = 1499/49 ms), was calculated for each preparation and scaling. The inverse of the SD values was used as a metric for noise sensitivity, and compared with simulations.

B^+_1 mapping linearity was assessed for the optimized preparation with $\phi_{TB} = 0$, and compared to subadiabatic HS8-sensitization. For the proposed BSS-prepared method, the same imaging parameters were used, as listed above, with the exception of flip angle (60°). The HS8 pulse mapping method was performed using the same pulse parameters as in simulations and acquired with a spoiled gradient echo (GRE) readout (flip angle = 7°, TR/TE = 2.7/1.2 ms, BW = 868 Hz/px, identical FOV/-matrix, centric k-space ordering). A 5-s rest period was used for the magnetization recovery between the non-prepared and HS8-sensitized images. For both mapping methods, B^+_1 inhomogeneities were simulated with scaling all RF between 5% and 100% in steps of 5%, acquiring two repetitions for each scale. B^+_1 inhomogeneities were simulated with scaling all RF between 5% and 100% in steps of 5%, acquiring two repetitions for each scale. The scale was normalized to the highest sensitivity point for both mapping methods, as determined from the simulations. In a manually drawn ROI in the central vial, the mean and standard deviation of the postpreparation signal ratio were compared to the simulations. The phantom data was compared to the simulations using linear regression and Bland–Altman analysis to determine an effective B^+_1 mapping range.

Noise resilience of the proposed method was compared with a conventional BSS mapping technique and the HS8-prepared technique in a torso-sized, cylindrical systems phantom. Images were acquired with the prepared BSS sequence (FOV = 450 × 450 mm^2, $s = 10$ mm, TR/TE = 1.99/0.94 ms), the conventional spoiled GRE BSS sequence (flip angle = 10°, TR/TE = 18/0.99 ms, BW = 1653 Hz/px, identical FOV/matrix) and the HS8-sensitized sequence (identical imaging parameters as above, TR/TE = 2.6/1.15 ms with matched FOV/matrix). For the conventional BSS sequence, 8 ms Fermi pulses were placed after each excitation, with 90% full-width-half-maximum, ±7 kHz off-resonance, and $B^+_{1,max} = 6.8$ μT to keep within SAR limits.[14] Ten image repetitions were acquired for the three methods to assess the mean and SD of the B^+_1 map within manually drawn ROIs.

2.5 | In vivo experiments

The study was ethically approved by the competent authority (METC: NL73381.078.20) and written informed consent was obtained from each subject prior to examination.

$|B^+_1|$ maps were acquired in four-chamber (4CH), two-chamber (2CH), and basal/mid/apical short axis orientations (SAXb, SAXm, SAXa) with two repetitions (FOV = 300 × 300 mm^2, $s = 10$ mm). Eleven subject data (seven female, 25±2 year old) were acquired for the proposed technique comparison with the conventional BSS mapping methods, and six subject data (female, 24 ± 3

year old) for the HS8-sensitization comparison. The conventional BSS technique used a segmented acquisition (TR/TE = 18/1.22–1.33 ms, BW = 1653 Hz/px) with 7–13 k-space lines per heartbeat triggered to the end-diastole in a single breath-hold. Sequential acquisition of all positive off-resonance shift lines, followed by all negative ones was performed. Fermi pulse parameters were equivalent to phantom imaging, with 5.9–7.6 μT amplitude. The HS8-prepared technique used imaging parameters equivalent to the phantom experiments (TR/TE = 2.7–2.8/1.2–1.3 ms with matched FOV/matrix) and a single-shot readout, with end-diastole triggered breath-hold acquisition. The conventional BSS, HS8-prepared and the proposed sequences resulted in 11–16, 7–8, and 8–9 s breath-holds, respectively. For all techniques, baseline image registration was performed in a group-wise manner using principal component analysis.[24] Based on a magnitude image ($I_{0\phi}$ for the proposed technique and HS8-prepared image for the HS8-sensitization), the real/imaginary parts of the baseline images were registered to this template.

Test–retest repeatability was measured as the absolute deviation between two sequence repetitions over a manually drawn ROI covering the whole heart. Additionally, the intersection lines between 4CH, 2CH, and SAXm planes were calculated and inspected for the proposed technique in twelve subjects (eight female, 25±2 year old).

Finally, the feasibility of a single 20-s breath-hold $|B_1^+|$ 3D mapping of the whole heart with the prepared sequence was demonstrated in one subject (female, 22 year old). The proposed sequence was modified to replace the rest period with a saturation pulse at the beginning of each RR cycle for magnetization reset. A segmented balanced steady-state free precession acquisition with 50 k-space lines per heartbeat was used, with flip angle = 30°, TR/TE = 2.5/1.2 ms, BW = 1447 Hz/px, FOV = 220 × 220 × 120 mm^3 and matrix size = 72 × 44 × 12 in SAX view, SENSE = 1.5 in slice and phase-encode directions. The preparation duration was 45 ms, d_{BS} = 3.6 ms and $B^+_{1,max}$ = 11.5 μT. Three-dimensional (3D) maps were reformatted for visual comparison to match the 2D imaging slices. Manually drawn ROIs were used for quantitative evaluation.

3 | RESULTS

3.1 | Simulations

Off-resonant pulse duration optimization for a target maximum $B^+_{1,norm}$ = 1.1 yielded an upper bound of d_{BS} = 4.6 ms at $\phi_{TB} = 0$. Optimal refocusing was achieved with $\xi = 8$ and f_{max} = 5400 Hz for the d_{REF} = 4 ms tanh/tan pulses (Figure S1). These parameters achieved an average preparation efficiency of 92.38% over the optimization range.

The comparison of the numerical noise sensitivity between HS8 and BSS-based preparations is shown in Figure 2A. HS8 pulse achieves better sensitivity in low $B^+_{1,norm}$ region, while the proposed method shows strongly improved sensitivity for the upper range of B_1^+ scaling ($B^+_{1,norm} > 0.64$).

Mean absolute reconstruction bias due to relaxation effects at T_1 = 250 ms was simulated as 0.033 ± 0.016/0.017 ± 0.008/0.013 ± 0.006 for T_2 = 50/100/150 ms, respectively (Figure 2B). The biggest bias is observed for B_1^+-scaling ≈0.5, where the bias reaches up to 5.2%. This is reduced for T_1 = 1500 ms, yielding 0.028 ± 0.016/0.009 ± 0.005/0.005 ± 0.003 for T_2 = 50/150/250 ms.

3.2 | Phantom experiments

The tailored preparations with varying peak B_1^+ mapping sensitivity were achieved by simulating the following parameters: d_{BS} = 10/9/8 ms, $\phi_{TB} = -40°/-70°/-90°$, and tip angle of 110°/100°/90°. The simulated/measured postpreparation signals $M_{4\phi}/M_{0\phi}$ are shown in Figure 2C, top plot. Experimental data indicates good agreement with simulations (mean difference of 0.05 ± 0.04) for all tailored preparations. As per the design, the highest simulated sensitivity was at $B^+_{1,norm}$ = 0.7/0.8/0.9, respectively (Figure 2C, middle plot). The mapping sensitivity obtained various RF scaling confirms the shifting maximum B_1^+ mapping sensitivity peak across the three preparations (Figure 2C, bottom plot). With increasing d_{BS} and ϕ_{TB}, better sensitivity is achieved at lower B_1^+ scales.

For both the HS8-sensitized and the proposed technique, phantom experiments show good linearity (Figure 3A). The proposed technique shows good linearity and small deviation between the reconstructed $B^+_{1,norm}$ and the input RF scaling, for $B^+_{1,norm} \geq 0.3$ ($y = 1.07x - 0.06$, mean absolute difference = 0.031 ± 0.022, Figure 3A), when using the default preparation ($\phi_{TB} = 0$). For $B^+_{1,norm} < 0.3$, mapping accuracy and precision strongly decrease, which coincides with poor refocusing efficiency (Figure S1). For the HS8-sensitized method, good linearity is maintained even for very low $B^+_{1,norm}$ scales (with $y = 0.92x + 0.04$ for $B^+_{1,norm} \geq 0.3$, mean absolute difference 0.018±0.025). However, an increasing underestimation is observed for high $B^+_{1,norm}$ scales, reaching up to 0.08.

In the cylindrical phantom, preparation-based B_1^+ maps appear visually more homogeneous than conventional BSS (Figure 3B), which displays off-resonance artifacts at the edge of the phantom. Meanwhile, the HS8-sensitized map displays minor fold-over artifacts, and BSS-prepared map shows no visually apparent artifacts. The mean SD with the proposed method (0.002 ± 0.001) was greatly reduced when compared to the conventional

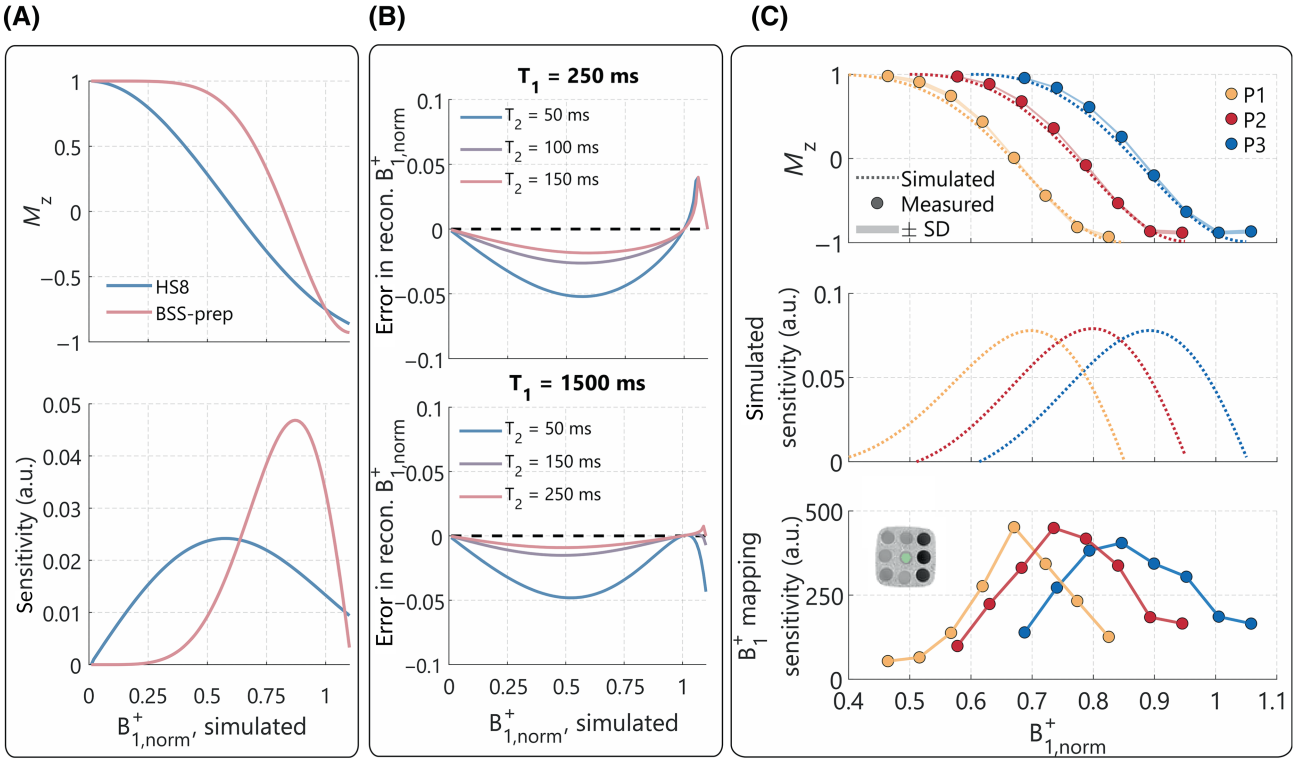

FIGURE 2 (A) Bloch-simulations of $|B_1^+|$ sensitizing preparations based on Bloch–Siegert shift (BSS), with $d_{BS} = 4.6$ ms Fermi pulses, 13.5 μT amplitude, and tip-back phase $\phi_{TB} = 0$ (red) and su-adiabatic hyperbolic-secant 8 (blue). The top panel shows the postpreparation magnetization as a function of the $|B_1^+|$ strength and the bottom panel shows the sensitivity, defined as the derivative of the postpreparation magnetization with respect to $B_{1,norm}^+$. Increased sensitivity is observed with BSS-based preparations for higher $|B_1^+|$ magnitudes ($|B_1^+| > 0.64$). (B) B_1^+ map reconstruction bias due to relaxation effects for various T_2 times in the presence of a short T_1 (top) and long T_1 (bottom). Small underestimation of less than 0.05 is observed, with the largest deviation occurring for $B_{1,norm}^+ > 1.0$ or $B_{1,norm}^+ \approx 0.5$. (C) B_1^+ mapping performance of three different preparations (P1, P2, and P3). The preparation parameters were tailored for different peak sensitivities, with Fermi pulse duration $d_{BS} = 10/9/8$ ms, tip-back phase $\phi_{TB} = -40°/-70°/-90°$, and tip angle of 110°/100°/90°, respectively. Postpreparation magnetization $M_{4\phi}/M_{0\phi}$ (top plot) shows good agreement between simulated data (dashed lines) and phantom (solid line). Mapping sensitivity in simulations (middle plot) and experiments (bottom panel) show comparable trends with a shift in peak sensitivity to higher B_1^+ values from P1 to P3. The phantom region of interest in the central vial is indicated in the bottom panel. (A) Mapping sensitivity; (B) Relaxation-induced error; (C) Preparation tailoring.

BSS mapping (0.048 ± 0.007), and slightly improved compared to the HS8-prepared method (0.004 ± 0.001).

3.3 | In vivo experiments

Images in subjects show visually improved B_1^+ mapping quality and uniformity in the proposed preparation-based mapping, particularly in comparison to the conventional BSS method (Figure 4A). While both preparation-based techniques achieve good mapping quality, the HS8-sensitization results in visually apparent tissue contrast. The characteristic trend of B_1^+ reduction toward the right ventricle and the apex is visible. The absolute test–retest difference was greatly reduced with the proposed technique when compared to the conventional BSS: from 0.135 ± 0.113/ 0.175 ± 0.135/ 0.134 ± 0.109/ 0.132 ± 0.110/ 0.147 ± 0.119 across all subjects for 4CH/2CH/SAXb/SAXm/SAXa orientations (0.140 ± 0.117 across all orientations), to 0.029 ± 0.041/ 0.033 ± 0.061/ 0.024 ± 0.036/ 0.023 ± 0.033/ 0.027 ± 0.045 (0.027 ± 0.043 across all orientations).Similar to phantom experiments, a slight improvement was achieved when compared to HS8-sensitized method: from 0.038 ± 0.044/ 0.035 ± 0.040/ 0.025 ± 0.030/ 0.044 ± 0.063/ 0.028 ± 0.043 (0.035 ± 0.047 across all orientations) to 0.024 ± 0.030/ 0.016 ± 0.017/ 0.018 ± 0.022/ 0.019 ± 0.026/ 0.022 ± 0.043 (0.020 ± 0.028 across all orientations). The SAR burden of the conventional BSS sequence was 2.6–2.7 W/Kg. The proposed BSS-prepared method yields a reduced SAR burden of 1.6–1.7 W/kg in the proposed sequence, despite the use of high flip angles in the balanced steady-state free precession readout. The HS8-prepared sequence with spGRE readout results in the lowest SAR burden (0.2 W/kg).

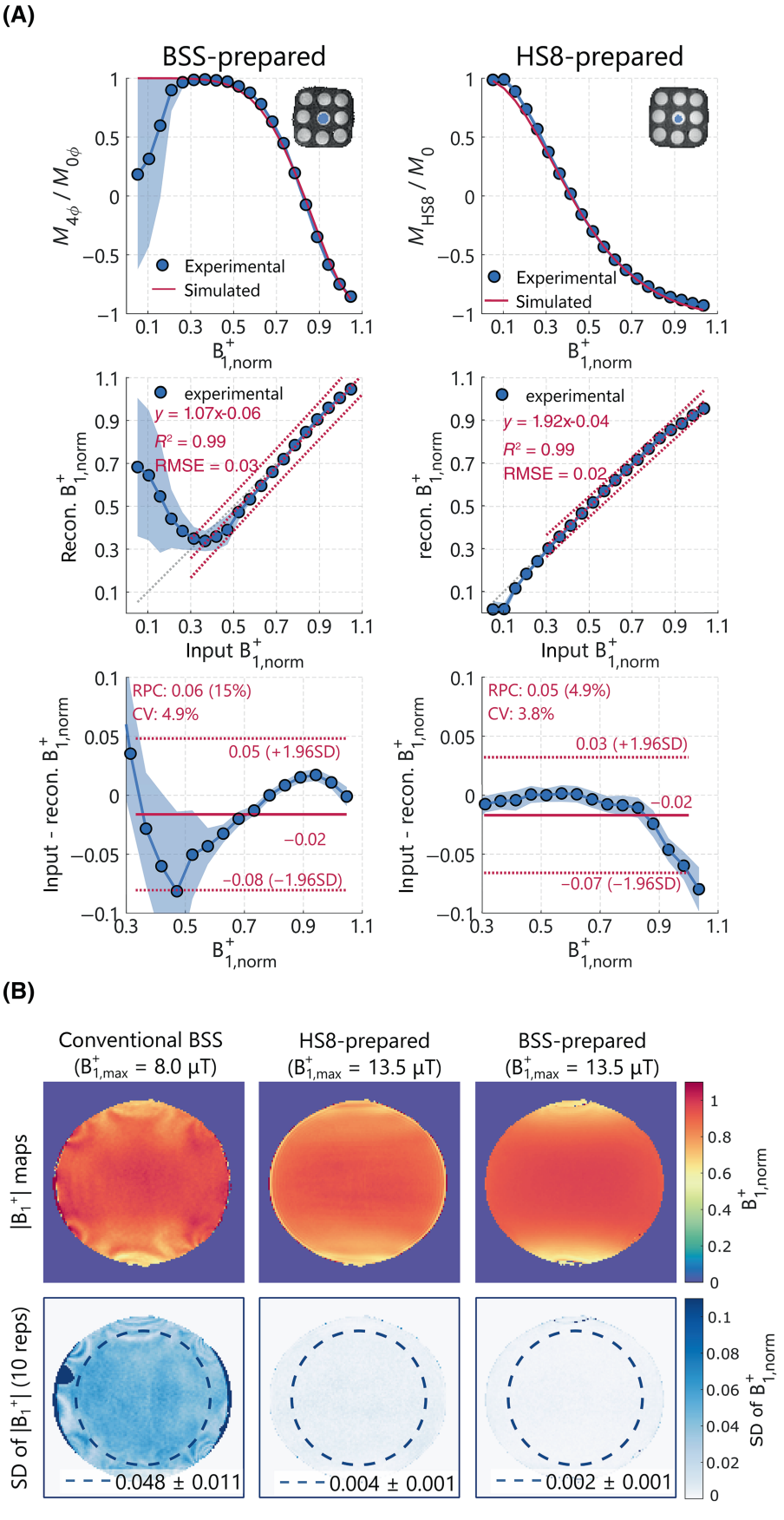

FIGURE 3 (A) Overlay of simulation and phantom results of the $|B_1^+|$ dependent signal using the proposed Bloch–Siegert shift (BSS)-preparation (left) with d_{BS} = 4.6 ms Fermi pulse duration, $B^+_{1,max}$ = 13.5 μT and ϕ_{TB} = 0, and the hyperbolic-secant 8 (HS8)-sensitization (right). The top plots illustrate postpreparation longitudinal magnetization ratio $M_{4\phi}/M_{0\phi}$ and M_{HS8}/M_0, while the middle plots show radiofrequency (RF) scaling and reconstructed B_1^+ linearity (left and) and bottom—the corresponding Bland–Altman analysis. (B) B_1^+ maps in the cylindrical phantom obtained using the conventional BSS mapping sequence (top left), the HS8-sensitization (top middle) and the proposed BSS-prepared method (top right). The corresponding SD maps from ten measurements are illustrated in the bottom row, with mean values over the region of interest (dashed line) of 0.048 ± 0.007 for the conventional BSS, 0.046 ± 0.001 for the HS8-sensitization, and 0.002 ± 0.001 for the proposed method. (A) RF scaling in T1MES phantom; (B) $|B_1^+|$ and SD maps.

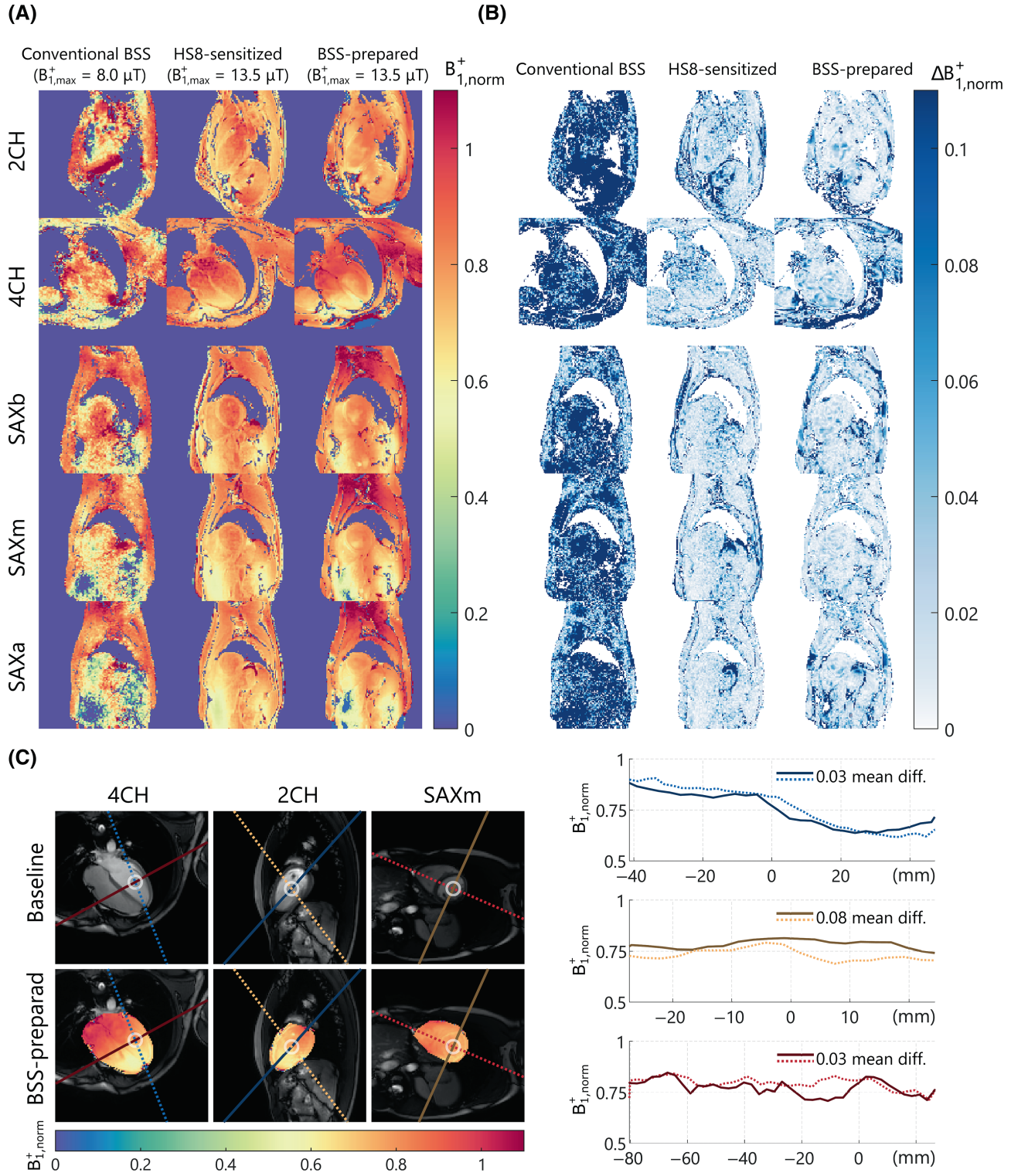

FIGURE 4 (A) B_1^+ maps of a representative subject for the conventional phase-based Bloch–Siegert shift (BSS) sequence (left column), the HS8-sensitized sequence (middle column) and the proposed BSS-prepared mapping sequence (right column), for five different orientations. (B) Corresponding maps of the absolute test–retest deviation. (C) B_1^+ map intersection analysis example for another subject. Imaging views are shown on the left side with baseline image and intersection line illustration (top) in blue (4CH-2CH), yellow (2CH-SAXm), and red (4CH-SAXm) lines. The bottom plots illustrate the BSS-preparation-based B_1^+ maps overlayed on the manually drawn heart ROIs. B_1^+ map intersection lines are plotted on the right side for a single subject. Across all subjects, the resulting mean absolute deviation values were 0.063 ± 0.052, 0.070 ± 0.030 and 0.046 ± 0.022 for 4CH-2CH, 2CH-SAXm and 4CH-SAXm intersections, respectively. (A) Representative subject $|B_1^+|$maps; (B) Test-retest repeatability; (C) Map intersection comparison.

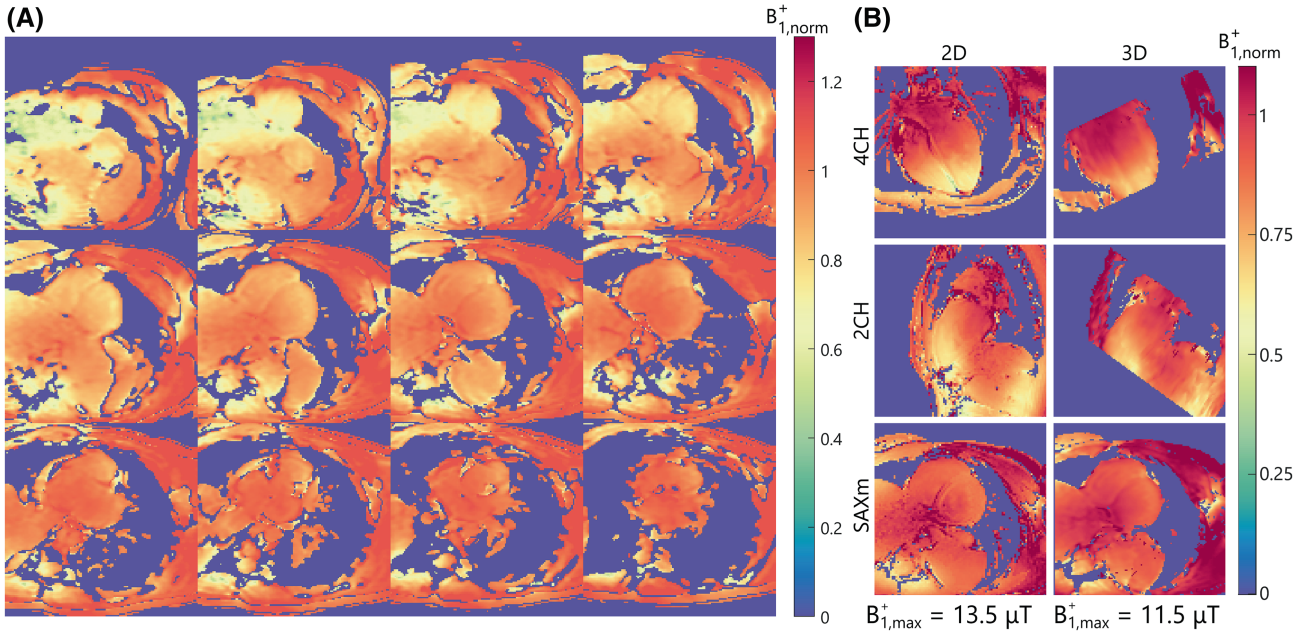

FIGURE 5 (A) Reconstructed three-dimensional (3D) B_1^+ maps in the short axis view, obtained using the modified Bloch–Siegert shift (BSS)-prepared sequence. (B) A side-by-side comparison of two-dimensional (2D) and a reformatted 3D B_1^+ map reconstructions in 4CH (top), 2CH (middle), and SAXm (bottom) orientations, with 2D maps cropped to reduced field of view to match the 3D acquisition. The mean absolute difference between the reformatted 2D and 3D maps was measured as 0.075 ± 0.065/0.168 ± 0.254/0.057 ± 0.135 for 4CH/2CH/SAXm orientations. (A) 3D prepared $|B_1^+|$ map ($B^+_{1,max} = 11.5\mu T$); (B) 2D/3D $|B_1^+|$ map comparison.

Figure 4C illustrates 4CH/2CH/SAXm intersection of the B_1^+ maps for a representative subject. Inspection reveals good overall agreement between different imaging planes, with a mean absolute difference of 0.050 ± 0.039/0.054 ± 0.028/0.050 ± 0.027 in 4CH-2CH, 2CH-SAXm, and 4CH-SAXm comparisons, respectively, across all subjects (0.052 ± 0.031 across all orientations).

The 3D acquisition shows good visual mapping quality (Figure 5A). A comparison between 2D maps and reformatted 3D imaging shows good agreement, with an absolute mean difference of 0.075 ± 0.065/0.168 ± 0.254/0.057 ± 0.135 for 4CH/2CH/SAXm views (0.055 ± 0.061 across all orientations), across the ROIs (Figure 5B).

4 | DISCUSSION

In this study, a cardiac B_1^+ mapping sequence based on BSS preparations was introduced and investigated at 3 T. The proposed preparation allowed for tailorable B_1^+ mapping sensitivity, and demonstrated strongly improved mapping quality compared with phase-based BSS mapping, and less relaxation-induced reconstruction bias compared with subadiabatic HS8 pulse-based preparation. Phantom results show good mapping accuracy down to 30% of the maximum B_1^+. In-vivo data indicate robust and efficient mapping of the B_1^+ transmit field magnitude at 3 T in 2D and 3D measurements.

B_1^+ mapping with the proposed preparation parameters is particularly sensitive to the upper range of B_1^+ values. This offers better sensitivity in the inhomogeneity range of interest at 3 T. In contrast, previously used preparations with sub-adiabatic HS8 pulses showed the highest sensitivity to low B_1^+, which may be less desirable.[19] In the proposed BSS-preparation, the tip-back phase ϕ_{TB} and Fermi pulse amplitude can be tailored to increase mapping sensitivity at lower B_1^+ areas. This may be useful for ultra-high field imaging, where the inhomogeneity range is expected to increase.

The main sensitization mechanism in the proposed preparation is based on the phase shift of the transverse magnetization. However, the use of hard pulses for tipping introduces sensitivity to B_1^+ inhomogeneities. This results in a mixed contrast, introducing a square cosine component in Equation (2). This factor can be avoided by implementing more robust tipping, such as adiabatic B_1-insensitive rotation pulses, albeit at the cost of increased sequence SAR. Imperfect tipping introduces a slight dependence on the relaxation effects. Due to the compensation intrinsic to the imaging scheme, this residual effect was neglected in B_1^+ reconstruction. Numerical simulations have shown that the T_1/T_2 relaxation-induced error does not exceed 5.2% under realistic conditions. However, evaluation of various tip down/up pulses, for a trade-off between SAR, a simplified reconstruction, and increased resilience

against residual relaxation remains the subject of future work.

Compared with conventional BSS-based B_1^+ mapping, the proposed sequence employs a lower number of off-resonant pulses. This allowed for a shorter TE, increasing off-resonance artifact resilience, as evident from the systems phantom acquisitions. Additionally, it reduces the SAR burden, and, importantly, decouples the B_1^+ sensitization from the readout. As a result, the proposed approach is suitable for increased spatial resolution or coverage. While these benefits are also offered by lower-SAR HS8-sensitization, the lack of $T_1\rho$ relaxation compensation during the subadiabatic pulse results in a significant tissue contrast. The spoiled GRE readout, used in HS8-sensitization, could be considered in the proposed sequence to enable lower SAR.

To enable whole heart coverage with 3D imaging in a single breath-hold, the proposed mapping sequence was modified to replace the rest period with a saturation pulse at the beginning of each RR cycle. The visual map quality of the acquired 3D maps proved to be largely satisfactory, indicating sufficient noise resilience. However, the rest periods enable higher signal-to-noise ratio due to more robust imaging readouts with lower parallel imaging factors, as evident by the direct 2D–3D comparison. In addition, imperfect saturation in the presence of low B_1^+ may compromise the mapping accuracy. Thus, the use of saturation or rest periods presents a viable trade-off between spatial coverage, scan time efficiency, and noise resilience.

The proposed B_1^+ mapping method and this study have several limitations. Firstly, hard tip-down/tip-up pulses are compromised in the presence of strong B_0 inhomogeneities, leading to a bias in B_1^+ reconstruction. The quantification of this bias, as well as a search for alternative and more robust tipping pulses warrants future investigation. Similarly, strong B_1^+ inhomogeneities lead to incomplete refocusing and saturation, limiting the effective B_1^+ mapping range. This is particularly relevant for ultra-high magnetic field applications (7 T and above), where further sequence optimization may be required for application to the increased range of B_1^+ inhomogeneities. Finally, only a small dataset of healthy subjects was presented in this work. To further establish clinical robustness and mapping reproducibility, investigation in a larger cohort of clinical patients is warranted.

Different applications of B_1^+ mapping can have divergent requirements on the B_1^+ map resolution, coverage, and noise resilience. While multi-transmit coil shimming can be performed at relatively low resolution and signal-to-noise ratio, quantitative map corrections require higher signal-to-noise ratio to avoid compromising the quantification precision. Emerging applications such as cardiac Electrical Properties Tomography[25,26] require even higher noise resilience to cater to spatial derivatives that are highly susceptible to noise. In the proposed technique, tailored preparations and acquisition parameters enable different trade-offs between noise resilience, bias, and coverage. Further investigation in the context of specific B_1^+ mapping applications is warranted to further optimize the B_1^+ map quality.

5 | CONCLUSIONS

In this study, a BSS preparation-based B_1^+ mapping sequence was investigated for cardiac application. The preparations allow for customization of the B_1^+ mapping sensitivity, with particularly good sensitivity at high B_1^+ values. Excellent map quality was demonstrated in phantom and in-vivo experiments at 3 T across the inhomogeneity range, with robust mapping extension to 3D imaging of the whole heart. When compared to phase-based BSS imaging, the proposed sequence achieved greatly reduced noise and visually improved mapping quality. Thus, the proposed method is a promising candidate for robust B_1^+ mapping for various applications at high fields.

FUNDING INFORMATION

This work is supported by the Nederlandse Organisatievoor Wetenschappelijk Onderzoek (STU.019.024); the 4TU Precision Medicine program supported by High Tech for a Sustainable Future; the Nederlandse Hartstichting (Dekker Grant, 03-004-2022-0079), the European Research Council (ERC StG, VascularID, 101078711).

CONFLICT OF INTEREST STATEMENT

The authors declare no potential conflict of interests.

ORCID

Paulina Šiurytė https://orcid.org/0000-0002-5806-8679
Joao Tourais https://orcid.org/0000-0002-1388-4023
Yi Zhang https://orcid.org/0000-0003-0523-3877
Chiara Coletti https://orcid.org/0000-0001-5994-2834
Stefano Mandija https://orcid.org/0000-0002-4612-5509
Markus Henningsson https://orcid.org/0000-0001-6142-3005
Sebastian Weingärtner https://orcid.org/0000-0002-0739-6306

REFERENCES

1. Shantha RP, François Christopher J, Tim L. Cardiac MRI: state of the art. *Radiology*. 2023;307:e223008.
2. Kramer CM, Barkhausen J, Bucciarelli-Ducci C, Flamm SD, Kim RJ, Nagel E. Standardized cardiovascular magnetic

resonance imaging (CMR) protocols: 2020 update. *J Cardiovasc Magn Reson*. 2020;22:1-18.
3. Wen H, Denison TJ, Singerman RW, Balaban RS. The intrinsic signal-to-noise ratio in human cardiac imaging at 1.5, 3, and 4 T. *J Magn Reson*. 1997;125:65-71.
4. Bernstein Matt A, John HIII, Ward HA. Imaging artifacts at 3.0 T. *J Magn Reson Imaging*. 2006;24:735-746.
5. Wieben O, Francois C, Reeder SB. Cardiac MRI of ischemic heart disease at 3 T: potential and challenges. *Eur J Radiol*. 2008;65:15-28.
6. Greenman RL, Shirosky JE, Mulkern RV, Rofsky NM. Double inversion black-blood fast spin-echo imaging of the human heart: a comparison between 1.5 T and 3.0 T. *J Magn Reson Imaging*. 2003;17:648-655.
7. Sung K, Nayak KS. Measurement and characterization of RF nonuniformity over the heart at 3T using body coil transmission. Journal of magnetic resonance imaging: an official journal of the international society for. *Magn Reson Med*. 2008;27:643-648.
8. Buonincontri G, Sawiak SJ. MR fingerprinting with simultaneous B1 estimation. *Magn Reson Med*. 2016;76:1127-1135.
9. Boudreau M, Tardif CL, Stikov N, Sled JG, Lee W, Pike GB. B1 mapping for bias-correction in quantitative T1 imaging of the brain at 3T using standard pulse sequences. *J Magn Reson Imaging*. 2017;46:1673-1682.
10. Hoult DI, Phil D. Sensitivity and power deposition in a high-field imaging experiment. *J Magn Reson Imaging*. 2000;12:46-67.
11. Pohmann R, Scheffler K. A theoretical and experimental comparison of different techniques for B1 mapping at very high fields. *NMR Biomed*. 2013;26:265-275.
12. Cunningham CH, Pauly JM, Nayak KS. Saturated double-angle method for rapid B1+ mapping. *Magn Reson Med*. 2006;55:1326-1333.
13. Clarke WT, Robson MD, Rodgers CT. Bloch-Siegert-mapping for human cardiac 31P-MRS at 7 tesla. *Magn Reson Med*. 2016;76:1047-1058.
14. Weingärtner S, Zimmer F, Metzger GJ, Uğurbil K, van de Moortele PF, Akçakaya M. Moortele Pierre-Francois, Akçakaya Mehmet. Motion-robust cardiac mapping at 3T using interleaved Bloch-Siegert shifts. *Magn Reson Med*. 2017;78:670-677.
15. Sacolick LI, Wiesinger F, Hancu I, Vogel MW. B1 mapping by Bloch-Siegert shift. *Magn Reson Med*. 2010;63:1315-1322.
16. Nehrke K, Börnert P. DREAM—a novel approach for robust, ultrafast, multislice B1 mapping. *Magn Reson Med*. 2012;68:1517-1526.
17. Chung S, Kim D, Breton E, Axel L. Rapid B1+ mapping using a preconditioning RF pulse with TurboFLASH readout. *Magn Reson Med*. 2010;64:439-446.
18. Nehrke K, Börnert P. Fast B1 mapping using a STEAM-based Bloch-Siegert preparation pulse. *Proc Int Soc Mag Reson Med*. 2011;19:4411.
19. Kent JL, Dragonu I, Valkovič L, Hess AT. Rapid 3D absolute B1+ mapping using a sandwiched train presaturated TurboFLASH sequence at 7 T for the brain and heart. *Magn Reson Med*. 2023;89:964-976.
20. Ogg RJ, Kingsley RB, Taylor JS. WET, a T1-and B1-insensitive water-suppression method for in vivo localized 1H NMR spectroscopy. *J Magn Reson B*. 1994;104:1-10.
21. Tannús A, Garwood M. Adiabatic pulses. *NMR Biomed*. 1997;10:423-434.
22. Idiyatullin D, Corum C, Moeller S, Garwood M. Gapped pulses for frequency-swept MRI. *J Magn Reson*. 2008;193:267-273.
23. Captur G, Gatehouse P, Keenan KE, et al. A medical device-grade T1 and ECV phantom for global T1 mapping quality assurance—the T1 mapping and ECV standardization in cardiovascular magnetic resonance (T1MES) program. *J Cardiovasc Magn Reson*. 2016;18:58.
24. Tao Q, van der Tol P, Berendsen FF, Paiman EHM, Lamb HJ, van der Geest RJ. Robust motion correction for myocardial T1 and extracellular volume mapping by principle component analysis-based groupwise image registration. *J Magn Reson Imaging*. 2018;47:1397-1405.
25. Liu J, Wang Y, Katscher U, He B. Electrical properties tomography based on B1 maps in MRI: principles, applications, and challenges. *IEEE Trans Biomed Eng*. 2017;64:2515-2530.
26. Katscher U, Weiss S. Mapping electric bulk conductivity in the human heart. *Magn Reson Med*. 2022;87:1500-1506.

SUPPORTING INFORMATION

Additional supporting information may be found in the online version of the article at the publisher's website.

Figure S1. The results of the refocusing pulse (duration d_{REF} = 5 ms) parameter optimization for high B_0/B_1^+ resilience at $B_{1,norm}^+ \in [0.5,1.1]$ and off-resonance $\Delta\omega \in [-200,200]$ Hz using Bloch simulations of the preparation with $\phi_{BS} = 0$. (A) Mean post-preparation magnetization M_z plotted for a range of tanh/tan pulse parameters ξ and f_{max}. (B) The optimal refocusing yields $\xi = 8$ and f_{max} = 5.4 kHz with 0.9238 mean postpreparation magnetization over the optimization region (dashed).

How to cite this article: Šiurytė P, Tourais J, Zhang Y, et al. Preparation-based B_1^+ mapping in the heart using Bloch–Siegert shifts. *Magn Reson Med*. 2024;1-11. doi: 10.1002/mrm.30232